Transformation of stimulus value signals into motor commands during simple choice

Todd A. Hare[a,b,1], Wolfram Schultz[c], Colin F. Camerer[a], John P. O'Doherty[a], and Antonio Rangel[a]

[a]Computation and Neural Systems and Humanities and Social Science Divisions, California Institute of Technology, Pasadena, CA 91125; [b]Laboratory for Social and Neural Systems Research, Department of Economics, University of Zurich, 8006 Zurich, Switzerland; and [c]Department of Physiology, Development, and Neuroscience, Cambridge University, Cambridge CB2 1TN, United Kingdom

Edited* by William T. Newsome, Stanford University, Stanford, CA, and approved September 20, 2011 (received for review June 10, 2011)

Decision-making can be broken down into several component processes: assigning values to stimuli under consideration, selecting an option by comparing those values, and initiating motor responses to obtain the reward. Although much is known about the neural encoding of stimulus values and motor commands, little is known about the mechanisms through which stimulus values are compared, and the resulting decision is transmitted to motor systems. We investigated this process using human fMRI in a task where choices were indicated using the left or right hand. We found evidence consistent with the hypothesis that value signals are computed in the ventral medial prefrontal cortex, they are passed to regions of dorsomedial prefrontal cortex and intraparietal sulcus, implementing a comparison process, and the output of the comparator regions modulates activity in motor cortex to implement the choice. These results describe the network through which stimulus values are transformed into actions during a simple choice task.

dynamic causal modeling | valuation

Implementing a choice necessarily requires taking an action. Consider the problem faced by an individual that has to choose between two stimuli, one placed on the left and obtained through a left hand movement and one placed on the right and obtained through a right hand movement. Theoretical models and a growing body of evidence (1–3) suggest that the brain solves this task by assigning values to the two stimuli, comparing them, and then activating the necessary motor response to implement the choice. It follows that, to solve the choice problem, the brain needs to transform stimulus value signals into motor commands.

Over the last decade, we have learned a considerable amount about the encoding of stimulus value signals at the time of choice. Functional MRI (fMRI) studies have found stimulus value signals in ventromedial prefrontal cortex (vmPFC) at the time of decision-making for primary rewards (4–8), monetary gains and losses (9–14), delayed rewards (15), consumer goods (16, 17), and abstract social rewards (18, 19). Related studies using electrophysiological recordings in nonhuman primates have shown that stimulus values are encoded in the firing rates of individual neurons in the orbitofrontal cortex (20–23). Importantly, these studies have shown that these areas encode stimulus value signals that are independent of the actual choice made, suggesting that they are an input to the choice process, which is outlined in the framework above.

The values assigned to each option must be compared to select the best course of action. Exactly how this comparison occurs in the brain is an area of active research. One important clue comes from computational models of the choice process that have shown that the drift diffusion model (DDM) (24, 25) and some of its variants (26–29) fit the accuracy and reaction time data of simple choice tasks remarkably well. Furthermore, activity resembling the output of the DDM has been found in the lateral intraparietal cortex during perceptual decision-making tasks in nonhuman primates (30, 31) and the dorsal medial prefrontal cortex (dmPFC) during action selection tasks in humans (32).

Here, we seek to identify the network involved in transforming stimulus values into motor commands using fMRI. Our strategy relies on the fact that an area involved in the comparison process and linking value computation to action implementation should satisfy the following three properties. First, its blood oxygen level-dependent (BOLD) signal should reflect the predictions for aggregate activity derived from neural implementations of the DDM. This property is important, because the DDM has been shown to fit the psychometric data in this class of tasks extremely well (24, 25). Second, the region should exhibit increased effective connectivity from areas such as vmPFC that encode stimulus values at the time of choice. This property is important, because the comparator needs to receive the value signals to be able to make choices. Third, the region should exhibit choice-dependent effective connectivity with motor cortex in a way that promotes the observed motor responses: it should enhance activity in the left motor cortex during right actions and activity in the right motor cortex during left actions. Based on the evidence described above and the well-characterized connectivity between the dmPFC and supplemental motor areas (33–35), we hypothesized that dmPFC and intraparietal sulcus (IPS) would satisfy the three properties and thus, provide the link between vmPFC and motor cortex during the transformation of stimulus values into motor commands.

Previous studies have looked at individual aspects of the value transformation network but have never tested for all of the functions necessary to move from valuation to action. A recent fMRI study of human decision-making found that IPS activity was consistent with some of the properties that one would expect from a comparator process, including increased connectivity with vmPFC at the time of choice and greater activity for more difficult choices (36), and a previous study by our own group suggested that activity in dmPFC might reflect, in part, the computations of a comparator process (7). Another study (37) found that activity in vmPFC was stronger in easier trials than more difficult decision trials, which is consistent with the hypothesis that the vmPFC might be involved in the computation of relative stimulus values. Note that, although these papers are important precursors on which we build and their results are consistent with subsets of the results obtained here, none of them address the fundamental goal of fully characterizing the network involved in how value signals are transmitted to putative comparison regions and ultimately, modulate activity in motor cortex to implement the choice. In particular, none of them has examined the connectivity of the entire network to test the predicted intratrial-, choice-, time-, and direction-specific changes in

Author contributions: T.A.H., W.S., C.F.C., J.P.O., and A.R. designed research; T.A.H. performed research; T.A.H. and A.R. analyzed data; and T.A.H., W.S., C.F.C., J.P.O., and A.R. wrote the paper.

The authors declare no conflict of interest.

*This Direct Submission article had a prearranged editor.

[1]To whom correspondence should be addressed. E-mail: todd.hare@econ.uzh.ch.

This article contains supporting information online at www.pnas.org/lookup/suppl/doi:10.1073/pnas.1109322108/-/DCSupplemental.

coupling between each region of the network. Here, we test these predictions using dynamic causal modeling (DCM) to examine the modulation of specific connections at a neuronal timescale (inferred from a hemodynamic deconvolution of the BOLD signal) during the periods of stimulus valuation and action preparation. Consistent with our hypotheses, we found that signaling from vmPFC to comparator regions increases at the time of choice, and subsequently, signaling from comparator regions to motor cortex increases during action preparation in a choice-dependent manner.

Results

We tested these hypotheses using a paradigm in which, on every trial, thirsty human subjects were shown pairs of symbols representing various amounts of different liquid rewards on the left and right sides of the screen, and later, they pressed either the left or right thumbs to indicate their choice (Fig. 1*A*). After another brief delay, the chosen liquid was delivered to the subjects inside the scanner on each trial. The task is closely related to the tasks used in works by Padoa-Schioppa and Assad to investigate the coding of stimulus value in orbitofrontal cortex with nonhuman primates (20, 21, 38).

Behavioral Results. We estimated the value of each amount of every different juice from the behavioral data using the procedure described in *Materials and Methods*. The psychometric curve in Fig. 1*B* shows that these value estimates provide an accurate account of the choice behavior. A mixed effects logistic regression showed that subjects were highly responsive to the relative value of the two juices ($t_{18} = 8.05$, $P < 0.001$).

Estimation of the Neural DDM. We estimated a simple neural implementation of the DDM. The model is important for our analyses, because it makes predictions about the level of aggregate activity and thus, about the BOLD responses that should be observed in an area involved in the comparison of stimulus values with action selection. As illustrated in Fig. 2*A*, the standard DDM assumes that (*i*) a relative value signal measuring the estimated relative value in favor of the left stimulus is computed dynamically through a Gaussian Markovian process, with independent and identically distributed noise and a mean slope of integration proportional to the underlying true value of the left minus right items; (*ii*) the relative value signal starts at zero; and (*iii*) a choice is made when either the signal crosses the upper barrier (so that the left option is selected) or the lower barrier (so that the right option is selected). At this level of computational abstraction, the DDM model does not make testable predictions about the level of activity associated with the comparator process that can be used to identify an area involved in these computations using fMRI. To achieve this link, we specified the simplest possible plausible neural implementation of the DDM that matches well with its behavioral predictions (29) (Fig. 2*B* and *Materials and Methods*).

An advantage of this model, which we refer to as neural DDM (nDDM), is that it is fully characterized by three free parameters (integration slope, inhibition strength, and integration noise). We estimated the values of these parameters that maximized the match with the group psychometric choice function shown in Fig. 2*C*. We used the model and best-fitting parameters to compute the expected total level of activity in the comparator region for each trial as a function of the relative values of the left and right items as well as whether the best item was chosen. Fig. 2*D* depicts the average predicted level of activity that is used below to identify regions associated with value comparison and action selection. This variable measures the total level of predicted activity generated by both pools of neurons, which is the relevant signal for identifying the neural comparator using BOLD fMRI as long as the two pools of neurons are spatially intermingled. Previous studies have used difficulty or reaction times as a marker for putative comparator regions (36, 39–41). Fig. 2*D* and the analyses discussed below show that, although this assumption is a good approximation to the predictions of the nDDM, it leaves out useful information. This void can be seen from the fact that the predicted activity levels have different curvature and average levels in correct and error trials. As described below and in *SI Results*, these differences can be exploited to compare the relative fit of the nDDM with difficulty-based regressors.

Stimulus Value Representation. We estimated a parametric general linear model (GLM) of BOLD activity that allowed us to identify areas in which activity was correlated with various signals of interest. Using this model, we found that activity in vmPFC correlated with the sum of the values during the initial screen depicting the two options ($P < 0.05$, small-volume corrected) (Fig. 3*A* and Table S1). Post hoc analyses of this area showed that activity did not differ by stimulus identity [one-way ANOVA for liquid type: $F_{(3,72)} = 0.90$, not significant (n.s.)], location (paired *t* test between left and right values: $t_{(18)} = -1.40$, n.s.), or

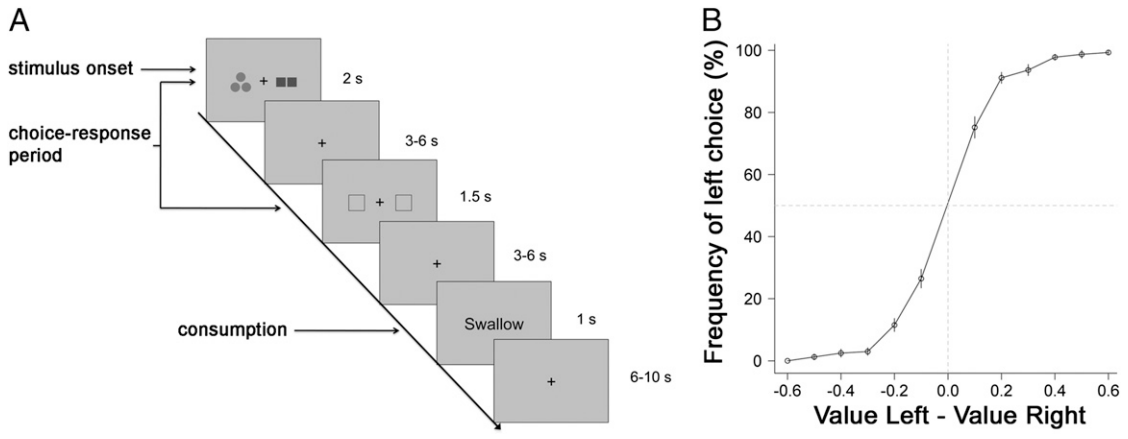

Fig. 1. Experimental design and behavior. (*A*) Subjects were presented with a choice screen offering two different amounts of two different liquids. Colored shapes represented the liquid identity. The number of shapes indicated the amount of liquid being offered. Subjects were instructed to make their choice while the shapes were on the screen, but they could only indicate their choice with a button press (left or right thumb) when the response prompt appeared after a variable delay period. The chosen stimulus was delivered after another variable delay period. (*B*) Percentage of left choices as a function of value of left minus value of right stimulus. Error bars represent the SEM across subjects.

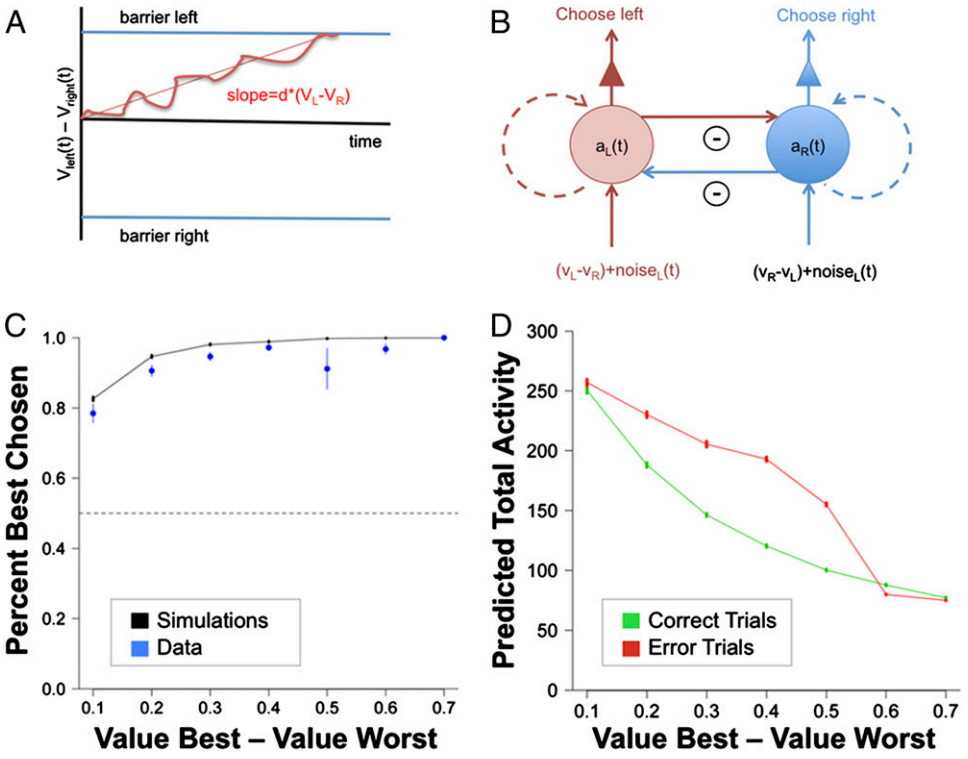

Fig. 2. Theoretical results. (*A*) Sketch of the basic DDM model of binary choice. (*B*) Summary of the neural implementation of the DDM. Red denotes activity encoding the relative value of left. Every instant *t*, this pool of neurons receives input ($V_L - V_R$) + error$_L(t)$, which is integrated to the previous level of activity $a_L(t)$ without leakage. The pool also receives a constant level of inhibition proportional to the level of activity in the right pool of neurons [denoted in blue; $a_R(t)$]. The dynamics for the system encoding the relative value of right are analogous. (*C*) Comparison of the psychometric choice curve for the group (blue) and the one generated by the model using the best-fitting parameters (black). (*D*) Total predicted activity (arbitrary units) in the comparator units (given by the sum of the instantaneous levels of activity in both pools of neurons up to the response time) as a function of the relative value of the two items and the correctness of the choice. Green, correct; red, incorrect. Error bars denote SE.

choice status (paired *t* test between chosen and nonchosen value: $t_{(18)} = 0.56$, n.s.).

Motor Responses. Next, we used the same GLM to identify activity associated with implementing specific motor responses. Left motor cortex (lMC) and right cerebellum were more active for responses with the right than the left thumb ($P < 0.05$, corrected) (Fig. S1*A* and Table S2). Conversely, right motor cortex (rMC) and left cerebellum were more active for responses with the left than right thumb ($P < 0.05$, corrected) (Fig. S1*B* and Table S2). Post hoc tests showed that lMC and rMC did not meet the criteria for encoding of action values (details in *SI Results*).

Comparator Regions Linking Valuation to Action: First Property. As described in the Introduction, any comparator region linking valuation to action in our experiment should satisfy three key properties. Here, we implement the test for the first property, which requires that BOLD responses at the time of stimulus presentation, when the choice is being made, correlate with the predicted total activity levels estimated from the nDDM, conditional on the relative value ($V^{best} - V^{worse}$) and the quality of choice (best chosen = 0, 1) in each trial (Fig. 2*D*). We found that activity in the dmPFC, left dorsolateral prefrontal cortex (dlPFC), and bilateral IPS correlated with this regressor during the period from stimulus onset through execution of the motor response ($P < 0.05$, corrected) (Fig. 3 *B* and *C*, Fig. S2, and Table S3).

Given the high correlation between the output of our nDDM and a measure of choice difficulty given by |value left − value right| ($r = -0.930$) and previous reports of correlations between dmPFC, dlPFC, and IPS with choice difficulty (42, 43), we performed post hoc Bayesian model selection on each region of interest to test whether the predictions from the nDDM or difficulty best explained activity in these regions. Note that, although there is a high correlation between the two measures, the nDDM predicts differences in the signal between correct and error trials that the difficulty measure does not predict. These differences can be exploited to test for the relative ability of each model to fit aggregate neural activity in areas of interest (additional details in *SI Results*). We used the exceedance probability (EP; the probability that a given model is more likely than any other model in the comparison set given the group data) as our metric for model comparison (44). The EP of the nDDM model was greater than the difficulty model in all four regions (dmPFC EP = 0.99, dlPFC EP = 0.58, lIPS EP = 0.98, and rIPS EP = 0.94), indicating that the nDDM provided a better fit to activity in these areas than the difficulty measure, especially in dmPFC and IPS.

Comparator Regions Linking Valuation to Action: Second and Third Properties. We next used DCM to investigate if the dmPFC, dlPFC, and IPS also exhibited the two key connectivity properties that an area involved in transforming stimulus values into motor commands should satisfy: (*i*) increased input at the time of choice from the region of vmPFC involved in computing stimulus values, and (*ii*) choice-dependent effective connectivity with motor cortex in a way that promotes the observed motor-responses.

First, we identified the most likely model using a Bayesian model selection process (*Materials and Methods*, *SI Materials and Methods*, and Tables S4–S10). The best model, depicted in Fig. 4, has reciprocal connections between vmPFC, dmPFC, dlPFC, and bilateral IPS and unidirectional connections from dmPFC, dlPFC, and bilateral IPS to lMC and rMC.

Second, after determining the most likely model, we used Bayesian parameter averaging to estimate the group posterior probabilities of each parameter of the best-fitting model. There are two types of parameters of interest in the model: fixed connection and coupling modulation parameters.

The fixed connection parameters measure the coupling between two areas during the rest periods of the task. There was a high posterior probability ($P > 90\%$) of fixed positive connections between most regions with the exception of vmPFC to dlPFC, dmPFC to lIPS, lIPS and rIPS to rMC, rIPS to lIPS, and

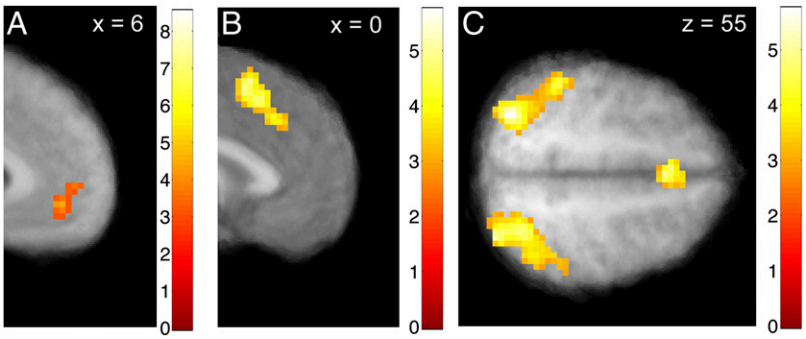

Fig. 3. Valuation and potential comparator regions. (*A*) Activity in vmPFC correlated with the sum of the stimulus values shown on each trial ($P < 0.05$, small-volume corrected). (*B* and *C*) Activity in bilateral dmPFC (*B*) and bilateral IPS (*C*) correlated with the predicted levels of activity generated by the nDDM model at $P < 0.05$, whole-brain corrected.

rMC to lMC (Table S5). There was also significant negative coupling from lMC to rMC.

The coupling modulation parameters measure how the interactions between regions change during specific phases of each decision trial. These modulation parameters represent our primary measure of interest in the DCM analysis, because they provide a direct test of the two properties of interest of comparator regions that might link valuation to action.

The first set of modulation parameters measures coupling changes during stimulus presentation, which coincides with the initial valuation and comparison of the two stimuli. We found that the coupling from vmPFC to dmPFC [$P(|\text{coupling } \Delta| > 0) = 0.93$] and left IPS [$P(|\text{coupling } \Delta| > 0) = 0.97$] and right IPS [$P(|\text{coupling } \Delta| > 0) = 0.95$] increased during this phase, which provides evidence in favor of the second criterion for these three areas (Fig. 4*B* and Table S6). Note that this increase in signaling from vmPFC to dmPFC and IPS was independent of the values of the options on each trial. This finding is to be expected, because the comparison process is necessary at all levels of value.

The second set of modulation parameters measures coupling changes during the period from stimulus onset to response for left and right choices separately. These parameters allowed us to estimate the posterior probabilities that the functional coupling strength depended on the identity of the chosen action, and thus, they help to test if IPS and dmPFC satisfy the third desired property. As described in Fig. 4 *C* and *D* and Tables S7 and S8, the functional coupling from dmPFC, dlPFC, and IPS to lMC and rMC was dependent on the choice. When the left action was chosen, there was positive modulation of the connections to rMC

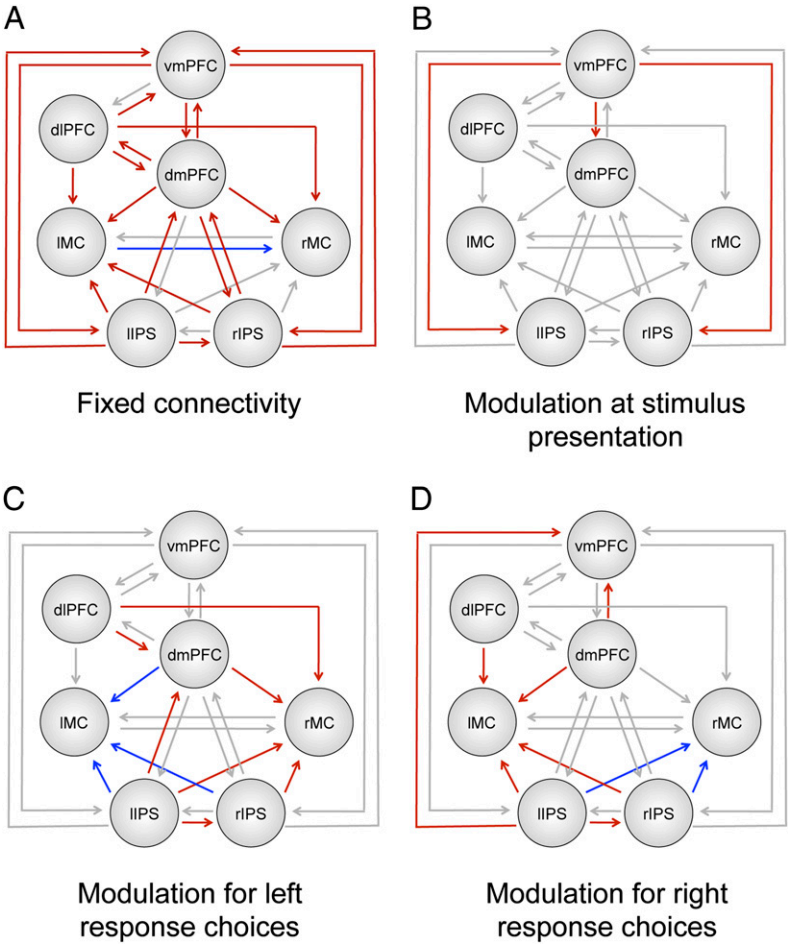

Fig. 4. Tests of functional coupling using DCM. (*A*) Diagram of the pattern of fixed connections between the seven regions in the most likely DCM model. Note that connections between dlPFC and IPS have been omitted for clarity but can be seen in Tables S1–S3. (*B*) Changes in connectivity during the stimulus valuation period. (*C*) Changes in connectivity during the period between stimulus onset and response in trials where subjects chose the left option. (*D*) Changes in connectivity during the period between stimulus onset and response in trials where subjects chose the right option. Connections in red indicate significant positive coupling coefficients, whereas blue indicates significant negative coefficients. Lines in gray indicate connections with posterior probability less than 90%.

from dmPFC [P(|coupling Δ| > 0) = 0.99], dlPFC [P(|coupling Δ| > 0) = 0.96], lIPS [P(|coupling Δ| > 0) = 0.92], and rIPS [P(|coupling Δ| > 0) = 0.97]. However, there was negative modulation of the connection to lMC from dmPFC [P(|coupling Δ| > 0) = 0.97], lIPS [P(|coupling Δ| > 0) = 0.97], and rIPS [P(|coupling Δ| > 0) = 0.93]. In contrast, during the period between stimulus presentation and right option selection, there was positive modulation of the coupling to lMC from dmPFC [P(|coupling Δ| > 0) = 0.99], dlPFC [P(|coupling Δ| > 0) = 98%], lIPS, and rIPS [P(|coupling Δ| > 0) = 0.99, whereas there was negative modulation of the connection to rMC from lIPS [P(|coupling Δ| > 0) = 0.96] and rIPS [P(|coupling Δ| > 0) = 0.94]. There was no significant modulation in coupling between lMC and rMC at the time of button press (Table S9). Together, these last findings provide evidence that dmPFC and IPS satisfy the third hypothesized property of a comparator region that links valuation to action.

Discussion

We have used a strategy to characterize the network involved in the transformation of stimulus values into a motor response during simple choice using fMRI. We found that activity in dmPFC and bilateral IPS exhibited three key properties that areas engaged in value comparison and linking choices to actions should satisfy. First, activity in these areas correlated with the predictions of a neural model of choice that approximates the computations of the DDM. This property is an important marker of comparator areas, because the DDM has been shown to fit the psychometric data from binary choice tasks (including ours) extremely well (24, 25). Second, our DCM analysis showed that activity in both areas exhibited increased functional coupling at the time of decision with the region of vmPFC that encoded both stimulus values, regardless of the choice that was eventually made. This increased coupling at the time of decision is expected in areas that use these value signals as inputs to the actual comparison process. Third, dmPFC and IPS exhibited choice-dependent coupling with motor cortex in a way that promoted the observed motor responses: they increased the connectivity with left motor cortex during right actions and with right motor cortex during left actions.

Our results provide a link between the value-based and perceptual decision literatures. Single-unit studies in nonhuman primates have found activity in IPS during saccadic dot motion tasks that resembles the output of a DDM comparator process (30, 31, 45, 46). Similar results have been obtained in human fMRI studies of perceptual decision-making (40, 41). Connections between vmPFC and parietal regions are likely to be polysynaptic. Therefore, future studies should seek to identify the intermediate nodes connecting vmPFC and parietal cortex in decision-making. One intriguing possibility is that the dmPFC and IPS might participate in the decision-making process by computing decision variables in the action and spatial domains, respectively. Unfortunately, in many paradigms, including our paradigm, the two types of decision variables are highly correlated and thus, are difficult to disentangle.

The dmPFC is a natural area to implement a comparison process in simple economic choice, because it is heavily interconnected with both supplementary motor areas and areas of vmPFC thought to be involved in valuation (33–35). Furthermore, neurons in dmPFC have been shown to reflect several different decision variables, making this region ideally qualified to compare different options and promote the best course of action (22).

Previous fMRI studies have shown that the dmPFC, dlPFC, and parietal cortex are more active in more difficult value-based decisions (42, 43). Given the high correlation between difficulty and the levels of activity predicted by the nDDM model, our results are consistent with these findings. However, we found that the nDDM model provides a better fit to activity in dmPFC and IPS, which is consistent with previous studies that have directly compared measures of difficulty and value differences in dmPFC (7).

In summary, our results provide evidence that a neural network, including regions of vmPFC that reflect stimulus value, comparator processes in dmPFC and IPS, and action effectors in motor cortex, mediates the transformation of stimulus values into motor commands at the time of choice. This transformation process is of central importance to decision neuroscience. A critical question for future investigations is to what extent the network identified here is at work in a wide class of decisions (encompassing many different stimulus types and effectors) or if, in contrast, the network linking stimulus valuation, value comparison, and motor action is dependent on the parameters of the task.

Materials and Methods

Participants. Twenty subjects (four females) participated in the experiment (mean age = 23 y, range = 19–35 y). All subjects were right-handed, were healthy, had normal or corrected to normal vision, had no history of psychiatric diagnoses or neurological or metabolic illnesses, and were not taking medications that interfered with the performance of fMRI. One male subject was excluded from analysis because of irregularities in his pattern of choices. The review board of the California Institute of Technology approved the study.

Stimuli and Task. Subjects completed a juice decision task in the MRI scanner (*SI Materials and Methods*). At the beginning of each trial, subjects saw two different flavor amount combinations—one on the left side and one on the right side of the screen (Fig. 1*A*). Subjects were instructed to make their choice while the left and right options were on the screen. After a variable delay (3–6 s), a response prompt was shown on the screen, and the subject pressed the right thumb to select the right option or the left thumb to select the left option. The chosen liquid was delivered to the subject after another variable delay (3–6 s). There were a total of 120 trials across the four functional runs. *SI Materials and Methods* has details of liquid reward value calculations.

Neural DDM. The model assumes that choices are made as follows every trial. There are two pools of neurons, which are spatially intermingled and of equal size, with total instantaneous levels of activity given by $a_L(t)$ and $a_R(t)$, where t indicated elapsed time from the appearance of the stimuli. At the beginning of the choice process, $a_L(0) = a_R(0) = 0$. A choice is made to the respective action when the level of activity in either of the two populations surpasses a prespecified threshold. The evolution equations for each population are given by (Eq. **1**)

$$a_L(t) = \max\{0, a_L(t-1) - \theta^* \; a_R(t-1) + d^*(v_L - v_R) + \eta_L(t)\} \qquad [1]$$

and (Eq. **2**)

$$a_R(t) = \max\{0, a_R(t-1) - \theta^* \; a_L(t-1) + d^*(v_R - v_L) + \eta_R(t)\} \qquad [2]$$

where θ measures the strength of the inhibitory activity between the two pools, d measures the sensitivity of the integration process to the underlying true values of the stimuli (denoted by v_L and v_R), and the last term, η, measures the measures the amplitude (SD) of Gaussian noise. We assume that the height of the barriers was fixed at ±1. Note that this normalization is without loss of generality, because the DDM is identified only up to relative values of the parameters. The psychometric curve for the best-fitting set of parameters ($d = 0.009 \pm 0.005$, $\eta = 0 \pm 0.035$, $\theta = 0.2$) is shown in Fig. 2*C*. Total activity in each trial predicted by the model is referred to as M_{out}. *SI Materials and Methods* has model estimation details.

The total activity shown in Fig. 2*D* was used as a modulator in some of the GLMs of BOLD activity described below to identify areas that might be associated with the comparison process. The logic for using this variable as a marker is described. BOLD activity in any instant in the comparator area should be proportional to the sum of local neural activity. It follows that average bold activity in this area from the time of stimulus onset to the time of decision should be proportional to the average of instantaneous activities. In the analyses below, we cannot modulate activity with duration equal to the reaction time, because our paradigm does not allow us to measure it. Instead, we model the activity of the comparator with an equal duration in all trials. By the previous arguments, average activity during this time should be proportional to the total level of activity.

fMRI Data Acquisition and Analysis. Data were acquired with a 3T scanner (Trio; Siemens) using an eight-channel phased array head coil (details in *SI Materials and Methods*). We estimated two GLMs with first-order autoregression for each individual subject (details in *SI Materials and Methods*). We then computed contrasts of interest at the individual level using linear combinations of the regressors. These contrast coefficients were used in one-sample *t* tests for second-level group analyses.

We carried out whole-brain corrections for multiple comparisons at the cluster level. Details of the correction for each contrast can be found in Tables S1–S11. Small-volume correction for the vmPFC was conducted within a 10-mm sphere centered on the vmPFC coordinates ($x, y, z = -3, 42, -6$) from the work by Chib et al. (16).

DCM. We examined the connectivity between stimulus value and motor response regions on left and right choice trials using DCM (47). The analysis was carried out in several steps.

First, seven activation time courses were extracted from the functional masks in vmPFC, dmPFC, dlPFC, lIPS, rIPS, lMC, and rMC in each subject from a 4-mm sphere centered on the individual subject peak within the group regions of interest identified by the main GLMs and shown in Fig. 3 and Figs. S1 and Figs. S2.

Second, we specified 20 different models of potential connectivity between the seven areas of interest. A full description of the set of models is provided in *SI Materials and Methods* and Tables S5–S10.

Third, we identified the best model using the Bayesian model selection method developed in the work by Stephan et al. (44) (Fig. S3). Briefly, this technique treats the models as random variables and computes a distribution of the probabilities for all models under consideration (additional details in *SI Materials and Methods*).

Fourth, we used Bayesian parameter averaging (details in *SI Materials and Methods*) (48, 49) to estimate the magnitudes and probabilities of each fixed connection (often called intrinsic connections) as well as the magnitudes and effects with which the connections are modulated by different events.

ACKNOWLEDGMENTS. We thank the Betty and Gordon Moore Foundation (C.F.C., J.P.O., and A.R.) for financial support as well as the National Science Foundation (A.R.).

1. Rangel A, Hare T (2010) Neural computations associated with goal-directed choice. *Curr Opin Neurobiol* 20:262–270.
2. Rushworth MF, Mars RB, Summerfield C (2009) General mechanisms for making decisions? *Curr Opin Neurobiol* 19:75–83.
3. Glimcher PW, Rustichini A (2004) Neuroeconomics: The concilience of brain and decision. *Science* 306:447–452.
4. Hare TA, Camerer CF, Rangel A (2009) Self-control in decision-making involves modulation of the vmPFC valuation system. *Science* 324:646–648.
5. Hare TA, O'Doherty J, Camerer CF, Schultz W, Rangel A (2008) Dissociating the role of the orbitofrontal cortex and the striatum in the computation of goal values and prediction errors. *J Neurosci* 28:5623–5630.
6. Plassmann H, O'Doherty J, Rangel A (2007) Orbitofrontal cortex encodes willingness to pay in everyday economic transactions. *J Neurosci* 27:9984–9988.
7. Wunderlich K, Rangel A, O'Doherty JP (2009) Neural computations underlying action-based decision making in the human brain. *Proc Natl Acad Sci USA* 106:17199–17204.
8. Rolls ET, Grabenhorst F, Parris BA (2010) Neural systems underlying decisions about affective odors. *J Cogn Neurosci* 22:1069–1082.
9. Tom SM, Fox CR, Trepel C, Poldrack RA (2007) The neural basis of loss aversion in decision-making under risk. *Science* 315:515–518.
10. Hampton AN, Bossaerts P, O'Doherty JP (2006) The role of the ventromedial prefrontal cortex in abstract state-based inference during decision making in humans. *J Neurosci* 26:8360–8367.
11. Levy I, Snell J, Nelson AJ, Rustichini A, Glimcher PW (2010) Neural representation of subjective value under risk and ambiguity. *J Neurophysiol* 103:1036–1047.
12. Rolls ET, McCabe C, Redoute J (2008) Expected value, reward outcome, and temporal difference error representations in a probabilistic decision task. *Cereb Cortex* 18: 652–663.
13. Kahnt T, Heinzle J, Park SQ, Haynes JD (2011) Decoding different roles for vmPFC and dlPFC in multi-attribute decision making. Neuroimage 56:709–715.
14. Blair K, et al. (2006) Choosing the lesser of two evils, the better of two goods: Specifying the roles of ventromedial prefrontal cortex and dorsal anterior cingulate in object choice. *J Neurosci* 26:11379–11386.
15. Kable JW, Glimcher PW (2007) The neural correlates of subjective value during intertemporal choice. *Nat Neurosci* 10:1625–1633.
16. Chib VS, Rangel A, Shimojo S, O'Doherty JP (2009) Evidence for a common representation of decision values for dissimilar goods in human ventromedial prefrontal cortex. *J Neurosci* 29:12315–12320.
17. Knutson B, Rick S, Wimmer GE, Prelec D, Loewenstein G (2007) Neural predictors of purchases. *Neuron* 53:147–156.
18. Hare TA, Camerer CF, Knoepfle DT, Rangel A (2010) Value computations in ventral medial prefrontal cortex during charitable decision making incorporate input from regions involved in social cognition. *J Neurosci* 30:583–590.
19. Smith DV, et al. (2010) Distinct value signals in anterior and posterior ventromedial prefrontal cortex. *J Neurosci* 30:2490–2495.
20. Padoa-Schioppa C, Assad JA (2008) The representation of economic value in the orbitofrontal cortex is invariant for changes of menu. *Nat Neurosci* 11:95–102.
21. Padoa-Schioppa C, Assad JA (2006) Neurons in the orbitofrontal cortex encode economic value. *Nature* 441:223–226.
22. Kennerley SW, Dahmubed AF, Lara AH, Wallis JD (2009) Neurons in the frontal lobe encode the value of multiple decision variables. *J Cogn Neurosci* 21:1162–1178.
23. Wallis JD, Miller EK (2003) Neuronal activity in primate dorsolateral and orbital prefrontal cortex during performance of a reward preference task. *Eur J Neurosci* 18: 2069–2081.
24. Ratcliff R, McKoon G (2008) The diffusion decision model: Theory and data for two-choice decision tasks. *Neural Comput* 20:873–922.
25. Smith PL, Ratcliff R (2004) Psychology and neurobiology of simple decisions. *Trends Neurosci* 27:161–168.
26. Usher M, McClelland JL (2001) The time course of perceptual choice: The leaky, competing accumulator model. *Psychol Rev* 108:550–592.
27. Krajbich I, Rangel A (2011) Multialternative drift-diffusion model predicts the relationship between visual fixations and choice in value-based decisions. *Proc Natl Acad Sci USA* 108:13852–13857.
28. Ditterich J (2006) Stochastic models of decisions about motion direction: Behavior and physiology. *Neural Netw* 19:981–1012.
29. Bogacz R (2007) Optimal decision-making theories: Linking neurobiology with behaviour. *Trends Cogn Sci* 11:118–125.
30. Gold JI, Shadlen MN (2007) The neural basis of decision making. *Annu Rev Neurosci* 30:535–574.
31. Shadlen MN, Newsome WT (2001) Neural basis of a perceptual decision in the parietal cortex (area LIP) of the rhesus monkey. *J Neurophysiol* 86:1916–1936.
32. Rowe JB, Hughes L, Nimmo-Smith I (2010) Action selection: A race model for selected and non-selected actions distinguishes the contribution of premotor and prefrontal areas. *Neuroimage* 51:888–896.
33. Beckmann M, Johansen-Berg H, Rushworth MF (2009) Connectivity-based parcellation of human cingulate cortex and its relation to functional specialization. *J Neurosci* 29: 1175–1190.
34. Picard N, Strick PL (2001) Imaging the premotor areas. *Curr Opin Neurobiol* 11: 663–672.
35. Strick PL, Dum RP, Picard N (1998) Motor areas on the medial wall of the hemisphere. *Novartis Found Symp* 218:64–75.
36. Basten U, Biele G, Heekeren HR, Fiebach CJ (2010) How the brain integrates costs and benefits during decision making. *Proc Natl Acad Sci USA* 107:21767–21772.
37. Rolls ET, Grabenhorst F, Deco G (2010) Choice, difficulty, and confidence in the brain. *Neuroimage* 53:694–706.
38. Padoa-Schioppa C (2009) Range-adapting representation of economic value in the orbitofrontal cortex. *J Neurosci* 29:14004–14014.
39. Heekeren HR, Marrett S, Ungerleider LG (2008) The neural systems that mediate human perceptual decision making. *Nat Rev Neurosci* 9:467–479.
40. Heekeren HR, Marrett S, Bandettini PA, Ungerleider LG (2004) A general mechanism for perceptual decision-making in the human brain. *Nature* 431:859–862.
41. Heekeren HR, Marrett S, Ruff DA, Bandettini PA, Ungerleider LG (2006) Involvement of human left dorsolateral prefrontal cortex in perceptual decision making is independent of response modality. *Proc Natl Acad Sci USA* 103:10023–10028.
42. Venkatraman V, Rosati AG, Taren AA, Huettel SA (2009) Resolving response, decision, and strategic control: Evidence for a functional topography in dorsomedial prefrontal cortex. *J Neurosci* 29:13158–13164.
43. Pochon JB, Riis J, Sanfey AG, Nystrom LE, Cohen JD (2008) Functional imaging of decision conflict. *J Neurosci* 28:3468–3473.
44. Stephan KE, Penny WD, Daunizeau J, Moran RJ, Friston KJ (2009) Bayesian model selection for group studies. *Neuroimage* 46:1004–1017.
45. Huk AC, Shadlen MN (2005) Neural activity in macaque parietal cortex reflects temporal integration of visual motion signals during perceptual decision making. *J Neurosci* 25:10420–10436.
46. Roitman JD, Shadlen MN (2002) Response of neurons in the lateral intraparietal area during a combined visual discrimination reaction time task. *J Neurosci* 22:9475–9489.
47. Marreiros AC, Kiebel SJ, Friston KJ (2008) Dynamic causal modelling for fMRI: A two-state model. *Neuroimage* 39:269–278.
48. Lee PM (1989) *Bayesian Statistics* (Oxford University Press, New York).
49. Kasess CH, et al. (2010) Multi-subject analyses with dynamic causal modeling. *Neuroimage* 49:3065–3074.

Supporting Information

Hare et al. 10.1073/pnas.1109322108

SI Results

Testing for Action Value Coding in Motor Cortex. Activity in both motor cortices increased as a function of the reward obtained by the selected action [i.e., the left motor cortex (lMC) positively correlated with the right value and the right motor cortex (rMC) positively correlated with the left value; $P < 0.05$, corrected] (Table S11).

Note, however, that lMC and rMC did not meet the criteria for the encoding of action values (1, 2), which is defined as a signal that encodes the value of an action regardless of whether it is chosen. Post hoc tests showed that, when the opposite response was chosen, lMC and rMC were not significantly correlated with right [$t_{(18)} = 1.21$, not significant (n.s.)] or left values ($t_{(18)} = -0.09$, n.s.), respectively.

Differences Between Neural Drift Diffusion Model Predictions of Total Activity in Comparator Regions and Difficulty Measures. Although these two measures are highly correlated, there are two important differences between them, which allows us to test which of the two parametric regressors fits better with the patterns of activity found in areas like dorsal medial prefrontal cortex (dmPFC) and intraparietal sulcus (IPS).

First, our neural drift diffusion model (nDDM) model predicts greater activity in comparator regions during error than correct trials (Fig. 2*D*), whereas the measure of difficulty does not differentiate between the two trial types. Here, we define an error trial as one in which the liquid of lower value is chosen. This greater activity in error than correct trials arises as a function of the noise and mutual inhibition parameters of the nDDM model.

Second, the difficulty measure is a simple linear function of the difference in values, whereas the activity predicted by the nDDM is monotonically related to the difference in values but not perfectly linear (Fig. 2*D*). This nonlinearity is present even when considering correct and error trials separately.

Motivated by these differences, we carried out a post hoc Bayesian model selection (3) in dmPFC, dorsolateral prefrontal cortex (dlPFC), and IPS to test whether the total activity measure from the nDDM or the difficulty measure best explained activity in these regions. We used the exceedance probability (EP; the probability that a given model is more likely than any other model in the comparison set given the group data) as our metric for model comparison. The EP of the nDDM model was greater than the difficulty model in all four regions (dmPFC EP = 0.99, dlPFC EP = 0.58, lIPS EP = 0.98, and rIPS EP = 0.94), indicating that the nDDM provided a better fit to activity in these areas than the difficulty measure, especially in dmPFC and IPS.

We ran an additional model comparison to determine whether the nDDM predictions were a better fit to blood oxygen level-dependent (BOLD) signals in dmPFC and IPS than difficulty, even when the distinction between correct and error trials was removed from the parametric regressor. To create this regressor, we assigned the parametric value of all trials as if they were correct. The all correct nDDM parametric regressor fit the BOLD signal better than difficulty (EP > 90%) in all regions of interest. However, the original nDDM regressor is also more likely than the all correct nDDM regressor (EP > 90%) in all regions of interest, indicating that both the shape of the curve and separation between correct and error trials are important factors in the fit to the BOLD signal.

There is also a previous body of literature suggesting that activity in the ventral parts of dmPFC, particularly in the anterior cingulate cortex (ACC), plays a role in resolving response conflict and error monitoring in a variety of tasks (4, 5). Although our results are not fundamentally incompatible with a role for ACC in error monitoring or response conflict in other paradigms, neither role is likely to explain the dmPFC activity in the current study. There are several reasons for this finding. First, the area of dmPFC identified here is more dorsal than the areas of ACC that have generally been associated with these alternative signals in previous studies. Second, response conflict in our paradigm would be the same as the choice difficulty measure discussed above. Third, error monitoring is also an unlikely function for dmPFC in our experiment, because we see the dmPFC become active well before the response (potentially an error) has been made.

SI Materials and Methods

Additional Stimuli and Task Details. Subjects abstained from all liquids for 3 h before the experiment. Before entering the scanner, subjects were asked to consume three saltine crackers to increase their level of thirst and were also given one saltine cracker to eat between the four functional runs to maintain thirst. Thirst ratings were obtained before each functional run to confirm that subjects remained thirsty throughout the task. A different colored shape represented each flavor (apple, grape, fruit punch, and water), with the number of shapes on the screen indicating the amount of liquid (1 = 0.2 mL, 2 = 0.45 mL, or 3 = 0.7 mL). If the subject failed to respond within 1.5 s after the response prompt appeared, an option was selected at random. Stimulus presentation, response recording, and liquid delivery were controlled using Cogent 2000 software (Wellcome Department of Imaging Neuroscience).

Liquid Delivery. Electronic syringe pumps located in the scanning control room delivered each liquid to the subject through ~10 m polyethylene tubing and a perfusion manifold. The perfusion manifold allowed four incoming tubes to be connected to one output tube with a minimum of dead space to avoid mixing the liquids. The subjects held the output tube between their lips like a straw while lying in the supine position inside the MRI scanner. Visual stimuli were presented using an overhead mirror and projection system.

Value of Liquid Rewards. We determined the subjective value of each liquid reward option using the individual's pattern of choices. The value of each flavor–amount combination was calculated using the equation $V = F \times A$, where V is the value of the option, F is the frequency with which that flavor was selected regardless of the amount offered, and A is the amount of liquid offered. All of the other value signals used in the analysis were derived from this basic calculation. In particular, the stimuli value (SV) for each trial was equal to the sum of the values for the available options (left value + right value). Action value left (right) was equal to the left (right) value. Chosen value (CV) was equal to the value of the chosen option, whereas nonchosen value (NCV) was equal to the value of the nonchosen option.

nDDM Estimation Procedure. The nDDM model assumes that the comparator system contains two identical pools of neurons: one encoding the relative value signal for left (i.e., value of left minus value of right) and one encoding the relative value signal for right (i.e., value of right minus value of left). The model also assumes that activity in each of the pools commences at a zero level and that each of them changes after a Gaussian Markovian process similar to the one for the DDM, except that they are not allowed to go below zero at any point during the decision process. Finally, the model assumes

that a choice is made in favor of its respective option when one of the two pools reaches a prespecified threshold level of activity and that the two pools dynamically inhibit each other.

We calibrated the model to the psychometric group choice data by simulating the model 5,000 times with different parameter sets and selecting the parameters that maximized the fit between the simulated and actual choice curves. Maximal fit was evaluated using a sum of square deviations criterion, including a weighting term for each level of $|V_L - V_R|$ that was inversely proportional to its frequency in the dataset. This calculation was done by searching among combinations of the following free parameters: mean and SD of the integration slope (d), SD of the Gaussian noise (η), and inhibition strength (θ). The psychometric curve for the best-fitting set of parameters ($d = 0.009 \pm 0.005$, $\eta = 0 \pm 0.035$, $\theta = 0.2$) is shown in Fig. 2*C*. We used the group choice data, because it leads to less noisy choice curves and therefore, generated more reliable estimates of the parameters of the nDDM.

We then used this set of parameters to estimate the distributions of total activity in both pools of comparator neurons by simulating the model 5,000 times for each combination of value differences. Total activity is defined to be as the sum of instantaneous levels of activity in both pools of neurons from stimulus onset to choice. Fig. 2*D* depicts summary statistics for the resulting distributions for both correct and error trials. The value of total activity in each trial predicted by the model is referred to as M_{out}.

We note one caveat to applying the nDDM to this dataset. Ideally, the experiment would have had free reaction times, which would have helped us to estimate the nDDM parameters more precisely, because the model makes predictions for both the accuracy and reaction time of choices. Because reaction time data are not available in our design, we fitted the nDDM using only the choice data. The lack of reaction time data likely introduces noise in our parameter estimates for the model and thus, reduces our ability to identify comparator regions using fMRI, but it does not introduce any systematic biases in our analyses.

Functional MRI Data Acquisition. The functional imaging was conducted using a Siemens 3.0 Tesla Trio MRI scanner. We acquired gradient echo T2*-weighted echoplanar images (EPIs) with BOLD contrast. To optimize functional sensitivity in the orbitofrontal cortex (OFC), we used a tilted acquisition in an oblique orientation of 30° to the anterior commissure–posterior commissure line (6). In addition, we used an eight-channel phased array coil that yields a 40% signal increase in signal in the OFC over a standard head coil. Each volume comprised 48 axial slices collected in an interleaved-ascending manner. Data were collected in four sessions (209 volumes, ~11 min). The imaging parameters were echo time, 30 ms; field of view, 192 mm; in-plane resolution and slice thickness, 3 mm; repetition time, 3 s. Whole-brain, high-resolution T1-weighted structural scans ($1 \times 1 \times 1$ mm) were acquired from the 20 subjects and coregistered with their mean EPI images; they were averaged together to permit anatomical localization of the functional activations at the group level.

Functional MRI Data Preprocessing. Image analysis was performed using SPM8 (Wellcome Department of Imaging Neuroscience). Images were corrected for slice acquisition time within each volume, motion-corrected, spatially normalized to the standard Montreal Neurological Institute EPI template, and spatially smoothed using a Gaussian kernel with a full width at one-half maximum of 8 mm. Intensity normalization and high-pass temporal filtering (using a filter width of 128 s) were also applied to the data.

General Linear Models. We estimated the following general linear model of BOLD responses to identify regions reflecting stimulus values, action values, and motor responses. This process was done in three steps.

First, for each individual, we estimated a general linear model (GLM) with first-order autoregression and the following nine indicator functions: R1, initial stimulus screen; R2, choice response period (CR); R3, left button press; R4, right button press; R5, juice delivery; R6–9, presence of each preference ranked juice (based on each subject's choices) on the stimulus screen. The stimulus screen, juice delivery, and preference ranked indicators were modeled as events with 1-s durations. The CR period was modeled as an event with duration equal to the elapsed time between the onset of the choice screen and the button press on that trial (5–9.5 s). Left and right button presses were modeled with durations equal to the reaction time as measured by the time elapsed between the appearance of the response screen and the button press. In addition to the nine indicator functions, the model included four parametric regressors: (*i*) choice screen × SV, (*ii*) CR × left V, (*iii*) CR × right V, and (*iv*) juice delivery × CV. The model also included session constants and motion parameters as regressors of no interest.

Second, we calculated first-level, single-subject contrasts for each of the four parametric regressors listed above.

Third, we calculated second-level group contrasts using one-sample t tests on the single-subject contrasts. We carried out whole-brain corrections for multiple comparisons at the cluster level. Details of the correction for each contrast can be found in Tables S1–S11. Small-volume correction for the ventromedial prefrontal cortex (vmPFC) was conducted within a 10-mm sphere centered on the vmPFC coordinates ($x, y, z = -3, 42, -6$) from the work by Chib et al. (7).

We estimated a second GLM to identify regions reflecting the output of our nDDM model. This model included the same indicator functions as the first GLM and the following parametric regressors: (*i*) choice screen × SV, (*ii*) CR × M_{out}, and (*iii*) juice delivery × CV. All omitted details are as detailed.

Post Hoc Analyses. To determine if stimulus location (left vs. right), choice (chosen vs. nonchosen), or identity (liquid 1–4) affected its association with vmPFC activity, we computed three additional GLMs. All of these GLMs included the same three indicator functions of (R1) choice screen, (R2) response screen, and (R3) juice delivery. The location model included parametric modulators for left V and right V for each indicator function. The choice model included parametric modulators for CV and NCV for each indicator function. There was little correlation between left value and right value (mean $r = -0.187$) or CV and NCV (mean $r = 0.183$). The identity model included parametric modulators for the value of each liquid for each indicator function. Liquid values were set to zero on trials where they were not offered.

First-level, single-subject contrasts were created for the parametric modulators left V, right V, chosen V, nonchosen V, and the value of each liquid at the time of choice screen onset. These single-subject contrast values were then averaged across all voxels shown in Fig. 3*A* and compared using paired t tests.

To test whether activity in dmPFC, dlPFC, and Par was more associated with M_{out} or difficulty (|left V − right V|), we estimated an additional GLM. This GLM was identical to the second GLM except that the parametric modulator for M_{out} from the previous model was replaced with |left V − right V|.

Post Hoc Comparison of Fits for nDDM and Difficulty GLMs. We created functional masks in dmPFC, dlPFC, and left and right Par from all voxels in those regions correlating with M_{out} and difficulty (conjunction threshold $P < 0.005$, uncorrected for each contrast). Next, we reestimated both GLMs using the Bayesian first-level estimation techniques incorporated into SPM8 and previously described in detail in the work by Penny et al. (8). Last, we used

a random effects Bayesian model selection procedure to determine exceedance probabilities that indicated whether the M_{out} or difficulty models provided a better fit to the data in each of the three regions. A brief description of this method is given in *Materials and Methods* on dynamic causal modeling, and additional details can be found in two recent papers (3, 9).

Dynamic Causal Modeling Description. For all 20 models tested, the driving inputs to all regions were assigned based on the results from the univariate GLMs and were not mean-centered (i.e., the fixed coupling parameters represent connectivity in the absence of task stimulation). Those inputs included five inputs: (*i*) an input of constant magnitude into vmPFC and dlPFC during stimulus presentation, (*ii*) an input to vmPFC during stimulus presentation proportional to the sum of the stimulus values, (*iii*) an input into dmPFC, dlPFC, and bilateral IPS of constant magnitude during the period from stimulus onset to button press for left choices, (*iv*) an input into dmPFC, dlPFC, and bilateral IPS of constant unit magnitude during the period from stimulus onset to button press for right choices, and (*v*) an input of constant value into lMC and rMC at the time of response. Parameter estimates for the inputs to each region are shown in Table S10. In addition, all of the models allowed for the following event-related changes in coupling strength: (*i*) the coupling from vmPFC to dmPFC, dlPFC, and parietal cortex was allowed to be influenced by the onset of the stimulus screen (unmodulated), (*ii* and *iii*) left and right CR periods were allowed to modulate coupling in all existing connections, and (*iv*) button presses were allowed to modulate self-connections in lMC and rMC. To carry out these analyses, we estimated an additional GLM that was identical to the first GLM described in *Materials and Methods* except that the CR period was separated into right and left choice trials, the choice screen was modeled with an indicator function of 2-s duration, and the indicators for each preference-ranked juice were omitted.

Bayesian Model Selection for Dynamic Causal Modeling. We identified the best model using the Bayesian model selection method developed by Stephan et al. (3). Briefly, this technique treats the models as random variables and computes a distribution of the probabilities for all models under consideration. The probabilities can be used to define a multinomial distribution over model space from which the likelihood that a specific model generated the data of a randomly selected subject can be estimated. This procedure permits the computation of the exceedance probability for each model in the comparison set, which measures the probability that each model is the most likely one to be correct. Note that the exceedance probabilities add to one over the comparison set and thus, generally decrease as the number of models considered increases. We posited 20 different models of connectivity involving the seven areas identified above (vmPFC, dmPFC, dlPFC, lMC, rMC, lIPS, and rIPS) and used a Bayesian model selection process to identify the most probable model in the set (Fig. S3). The set of alternative models is described in detail in Tables S5–S10. We specified a large set of models, because given existing data, we did not have strong priors about the exact pattern of connectivity in the network. The set of models considered included the model depicted in Fig. 4 and most variations where vmPFC, dlPFC, and IPS are disconnected from sets of one or two other regions, including motor cortex.

Bayesian Parameter Averaging. Here, we present the equations underlying the Bayesian parameter averaging method that we used to make inferences about the modulatory dynamic causal modeling parameters at the group level. As stated in the work by Kasess et al. (10) and in other works (11, 12), this procedure treats the posterior distribution for one subject as the prior for the next subject. The process continues up to the *n*th subject, resulting in the following expression (**S1**):

$$\begin{aligned} p(\theta|y_1,\ldots,y_N) &\propto p(\theta)\prod_{i=1}^{N} p(y_i|\theta) \\ &\propto p(\theta|y_1)\prod_{i=2}^{N} p(y_i|\theta) \\ &\propto p(\theta|y_1,\ldots,y_{N-1})\prod_{i=N}^{N} p(y_i|\theta) \end{aligned} \quad \textbf{[S1]}$$

Under Gaussian assumptions about the densities, which is the case in dynamic causal modeling, the procedure can be simplified using a reduced form, where subject-specific conditional parameter densities are weighted by their precision and summed across subjects (Eq. **S2**):

$$\mu = \Lambda^{-1}\sum_{i=1}^{N}\Lambda_i\mu_i \quad \textbf{[S2]}$$

and (Eq. **S3**)

$$\Lambda = \sum_{i=1}^{N}\Lambda_i \quad \textbf{[S3]}$$

where μ_i is the posterior mean of the *i*th subject and $\Lambda_I = \Sigma_i^{-1}$ is the inverse posterior covariance or precision matrix. The matrix Λ represents not only the precisions of the model parameters (on the diagonal) but also the interdependence of the parameters (off-diagonal elements). The incorporation of the within subjects estimation precision is an advantage of Bayesian parameter averaging over frequentist approaches (e.g., one-sample *t* test) that do not include any measure of within subject variance.

1. Lau B, Glimcher PW (2008) Value representations in the primate striatum during matching behavior. *Neuron* 58:451–463.
2. Wunderlich K, Rangel A, O'Doherty JP (2009) Neural computations underlying action-based decision making in the human brain. *Proc Natl Acad Sci USA* 106: 17199–17204.
3. Stephan KE, Penny WD, Daunizeau J, Moran RJ, Friston KJ (2009) Bayesian model selection for group studies. *Neuroimage* 46:1004–1017.
4. Botvinick MM (2007) Conflict monitoring and decision making: Reconciling two perspectives on anterior cingulate function. *Cogn Affect Behav Neurosci* 7:356–366.
5. Carter CS, van Veen V (2007) Anterior cingulate cortex and conflict detection: An update of theory and data. *Cogn Affect Behav Neurosci* 7:367–379.
6. Deichmann R, Gottfried JA, Hutton C, Turner R (2003) Optimized EPI for fMRI studies of the orbitofrontal cortex. *Neuroimage* 19:430–441.
7. Chib VS, Rangel A, Shimojo S, O'Doherty JP (2009) Evidence for a common representation of decision values for dissimilar goods in human ventromedial prefrontal cortex. *J Neurosci* 29:12315–12320.
8. Penny WD, Trujillo-Barreto NJ, Friston KJ (2005) Bayesian fMRI time series analysis with spatial priors. *Neuroimage* 24:350–362.
9. Rosa MJ, Bestmann S, Harrison L, Penny W (2010) Bayesian model selection maps for group studies. *Neuroimage* 49:217–224.
10. Kasess CH, et al. (2010) Multi-subject analyses with dynamic causal modeling. *Neuroimage* 49:3065–3074.
11. Neumann J, Lohmann G (2003) Bayesian second-level analysis of functional magnetic resonance images. *Neuroimage* 20:1346–1355.
12. Garrido MI, Kilner JM, Kiebel SJ, Stephan KE, Friston KJ (2007) Dynamic causal modelling of evoked potentials: A reproducibility study. *Neuroimage* 36:571–580.

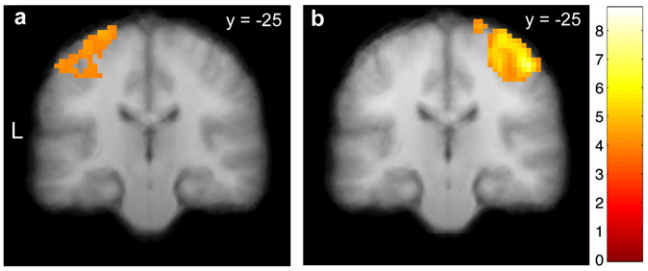

Fig. S1. Motor regions associated with left and right action selection. (*A*) Activity in the left motor cortex was greater when selecting the right juice reward with the right thumb than when selecting the left juice reward with the left thumb ($P < 0.05$, whole-brain corrected). (*B*) Activity in the right motor cortex was greater when selecting the left juice reward with the left thumb than when selecting the right juice reward with the right thumb ($P < 0.05$, whole-brain corrected).

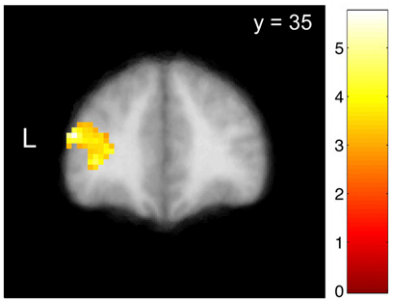

Fig. S2. Area of left dlPFC in which activity was also correlated with the predicted levels of activity generated by the nDDM at $P < 0.05$, whole-brain corrected.

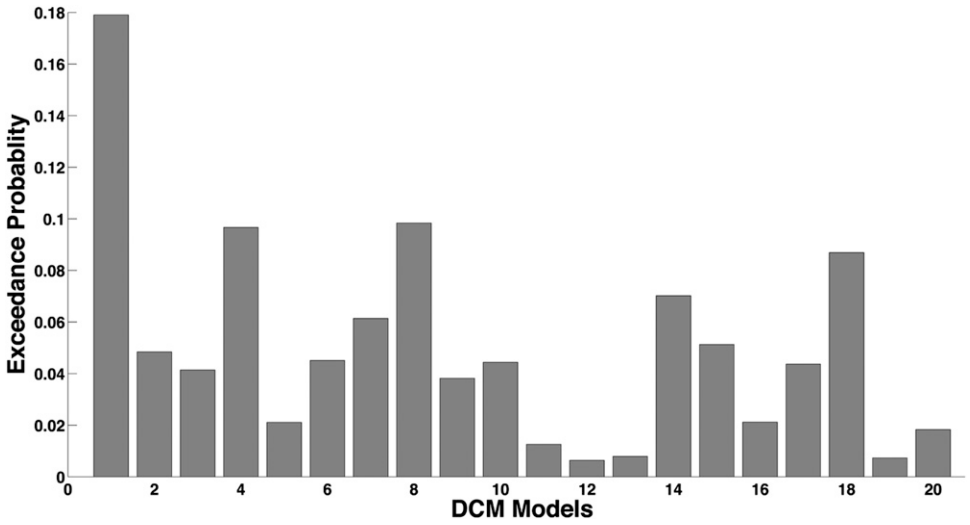

Fig. S3. Exceedance probabilities for the 20 alternative connectivity models. This measure represents the probability that each model is the most likely one to be correct among the set of models tested. The numbers on the *x* axis correspond to the numbering of the models in Table S4. The most probable model (dynamic causal model 1) is shown in Fig. 4 and Tables S5–S10.

Table S1. Regions correlating with stimulus values

Region	BA	Side	Cluster size	*x*	*y*	*z*	*Z* score
Occipital cortex	19/18	B	3,272	−18	−94	13	5.33*
Hippocampus		Left	37	−18	−25	−8	3.94
Hippocampus/amygdala		Right	47	12	−7	−11	3.72
Medial orbitofrontal/anterior cingulate cortex	10	Left	48	−6	44	−5	3.55†
Superior parietal lobule	7	Right	34	21	−70	46	3.37

Height threshold $t = 2.88$; extent threshold = 20 voxels (3 × 3 × 3 mm). BA, Brodmann area.
*The activation survives whole-brain correction for multiple comparisons at the cluster level (height threshold $t = 2.88$, extent = 134 voxels).
†Survives small-volume correction within a 10-mm sphere centered on the vmPFC coordinates ($x, y, z = -3, 42, -6$) from the work of Chib et al. (1).

1. Chib VS, Rangel A, Shimojo S, O'Doherty JP (2009) Evidence for a common representation of decision values for dissimilar goods in human ventromedial prefrontal cortex. *J Neurosci* 29: 12315−12320.

Table S2. Regions reflecting motor responses

Region	BA	Side	Cluster size	*x*	*y*	*z*	*Z* score
Regions showing greater responses for left vs. right responses							
Cerebellum		Left	968	−12	−52	−23	5.4*
Precentral gyrus	6/4/3	Right	1,188	42	−19	67	5.22*
Rolandic operculum/insula	13	Right	100	45	−19	19	3.99
Middle temporal gyrus	21	Left	44	−66	−43	−11	3.36
Putamen		Right	61	27	−10	4	3.3
Regions showing greater responses for right vs. left responses							
Precentral gyrus	4/3/6	Left	749	−45	−34	64	4.33*
Cuneus	18	Right	37	18	−97	7	3.75
Fusiform gyrus	19	Right	29	21	−64	−14	3.60
Cerebellum		Right	47	21	−49	−23	3.35

Height threshold $t = 2.88$; extent threshold = 20 voxels (3 × 3 × 3 mm). BA, Brodmann area.
*The activation survives whole-brain correction for multiple comparisons at the cluster level (height threshold $t = 2.88$, extent = 137 voxels).

Table S3. Regions reflecting the pattern of activity predicted by the DDM implementation

Region	BA	Side	Cluster size	*x*	*y*	*z*	*Z* score
Parietal cortex (IPS)	40/7	Left	483	−30	−70	55	4.27*
Insula	13/47	Left	53	−30	17	4	4.21
Middle/inferior frontal gyrus	46/10	Left	364	−51	35	19	4.17*
Parietal cortex (IPS)	40/7	Right	379	30	−49	40	3.92*
Medial frontal/cingulate gyrus	6/32	Right	193	0	14	58	3.86*
Inferior temporal lobe	37/20	Left	64	−54	−58	−17	3.82
Middle/inferior frontal gyrus	10/46	Right	125	42	41	10	3.77
Anterior cingulate cortex	24	Right	29	0	2	25	3.59
Precentral gyrus	6	Left	37	−45	−4	43	3.57
Lingual gyrus	18	Left	25	−12	−79	−8	3.55
Precentral gyrus	6	Left	32	−60	−10	40	3.47
Cerebellum		Left	95	−33	−67	−38	3.46
Inferior temporal lobe	17/18/19	Right	82	33	−70	−8	3.25
Precuneus	7	Right	23	12	−70	49	3.08
Thalamus		Left	27	−15	−13	13	3.07
Precuneus	7	Left	44	−6	−67	55	2.94
Posterior cingulate cortex	23	Right	20	6	−31	22	2.93

Height threshold $t = 2.88$; extent threshold = 20 voxels (3 × 3 × 3 mm). BA, Brodmann area.
*The activation survives whole-brain correction for multiple comparisons at the cluster level (height threshold $t = 2.88$, extent = 126 voxels).

Table S4. Alternative dynamic causal models tested

Region	*vmPFC* ⇒	*dmPFC* ⇒	*lIPS* ⇒	*rIPS* ⇒	*dlPFC* ⇒	*lMC* ⇒	*rMC* ⇒
DCM 1							
vmPFC	1	1	1	1	1	0	0
dmPFC	1	1	1	1	1	0	0
lIPS	1	1	1	1	1	0	0
rIPS	1	1	1	1	1	0	0
dlPFC	1	1	1	1	1	0	0
lMC	0	1	1	1	1	1	1
rMC	0	1	1	1	1	1	1
DCM 2							
vmPFC	1	0	1	1	1	0	0
dmPFC	0	1	1	1	1	0	0
lIPS	1	1	1	1	1	0	0
rIPS	1	1	1	1	1	0	0
dlPFC	1	1	1	1	1	0	0
lMC	0	1	1	1	1	1	1
rMC	0	1	1	1	1	1	1
DCM 3							
vmPFC	1	1	0	0	1	0	0
dmPFC	1	1	1	1	1	0	0
lIPS	0	1	1	1	1	0	0
rIPS	0	1	1	1	1	0	0
dlPFC	1	1	1	1	1	0	0
lMC	0	1	1	1	1	1	1
rMC	0	1	1	1	1	1	1
DCM 4							
vmPFC	1	1	1	1	0	0	0
dmPFC	1	1	1	1	1	0	0
lIPS	1	1	1	1	1	0	0
rIPS	1	1	1	1	1	0	0
dlPFC	0	1	1	1	1	0	0
lMC	0	1	1	1	1	1	1
rMC	0	1	1	1	1	1	1
DCM 5							
vmPFC	1	1	0	0	0	0	0
dmPFC	1	1	1	1	1	0	0
lIPS	0	1	1	1	1	0	0
rIPS	0	1	1	1	1	0	0
dlPFC	0	1	1	1	1	0	0
lMC	0	1	1	1	1	1	1
rMC	0	1	1	1	1	1	1
DCM 6							
vmPFC	1	1	1	1	1	0	0
dmPFC	1	1	0	0	1	0	0
lIPS	1	0	1	1	1	0	0
rIPS	1	0	1	1	1	0	0
dlPFC	1	1	1	1	1	0	0
lMC	0	1	1	1	1	1	1
rMC	0	1	1	1	1	1	1
DCM 7							
vmPFC	1	1	1	1	1	0	0
dmPFC	1	1	0	0	1	0	0
lIPS	1	1	1	1	1	0	0
rIPS	1	1	1	1	1	0	0
dlPFC	1	1	1	1	1	0	0
lMC	0	1	1	1	1	1	1
rMC	0	1	1	1	1	1	1
DCM 8							
vmPFC	1	1	1	1	1	0	0
dmPFC	1	1	1	1	0	0	0
lIPS	1	1	1	1	1	0	0
rIPS	1	1	1	1	1	0	0
dlPFC	1	0	1	1	1	0	0
lMC	0	1	1	1	1	1	1

Table S4. Cont.

Region	*vmPFC* ⇒	*dmPFC* ⇒	*lIPS* ⇒	*rIPS* ⇒	*dlPFC* ⇒	*lMC* ⇒	*rMC* ⇒
rMC	0	1	1	1	1	1	1
DCM 9							
vmPFC	1	1	1	1	1	0	0
dmPFC	1	1	0	0	0	0	0
lIPS	1	0	1	1	1	0	0
rIPS	1	0	1	1	1	0	0
dlPFC	1	0	1	1	1	0	0
lMC	0	1	1	1	1	1	1
rMC	0	1	1	1	1	1	1
DCM 10							
vmPFC	1	1	1	1	1	0	0
dmPFC	1	1	1	1	1	0	0
lIPS	1	1	1	1	1	0	0
rIPS	1	1	1	1	1	0	0
dlPFC	1	1	1	1	1	0	0
lMC	0	0	1	1	1	1	1
rMC	0	0	1	1	1	1	1
DCM 11							
vmPFC	1	1	1	1	1	0	0
dmPFC	1	1	1	1	1	0	0
lIPS	1	1	1	1	1	0	0
rIPS	1	1	1	1	1	0	0
dlPFC	1	1	1	1	1	0	0
lMC	0	1	0	0	1	1	1
rMC	0	1	0	0	1	1	1
DCM 12							
vmPFC	1	1	1	1	1	0	0
dmPFC	1	1	1	1	1	0	0
lIPS	1	1	1	1	1	0	0
rIPS	1	1	1	1	1	0	0
dlPFC	1	1	1	1	1	0	0
lMC	0	1	0	0	0	1	1
rMC	0	1	0	0	0	1	1
DCM 13							
vmPFC	1	1	1	1	1	0	0
dmPFC	1	1	1	1	1	0	0
lIPS	1	0	1	1	1	0	0
rIPS	1	0	1	1	1	0	0
dlPFC	1	0	1	1	1	0	0
lMC	0	1	0	0	0	1	1
rMC	0	1	0	0	0	1	1
DCM 14							
vmPFC	1	1	1	1	1	0	0
dmPFC	1	1	1	1	1	0	0
lIPS	1	1	1	1	0	0	0
rIPS	1	1	1	1	0	0	0
dlPFC	1	1	0	0	1	0	0
lMC	0	1	1	1	1	1	1
rMC	0	1	1	1	1	1	1
DCM 15							
vmPFC	1	1	0	0	1	0	0
dmPFC	1	1	1	1	1	0	0
lIPS	1	1	1	1	1	0	0
rIPS	1	1	1	1	1	0	0
dlPFC	1	1	1	1	1	0	0
lMC	0	1	1	1	1	1	1
rMC	0	1	1	1	1	1	1
DCM 16							
vmPFC	1	1	1	1	1	0	0
dmPFC	1	1	1	1	1	0	0
lIPS	1	1	1	1	1	0	0
rIPS	1	1	1	1	1	0	0

Table S4. Cont.

Region	*vmPFC* ⇒	*dmPFC* ⇒	*lIPS* ⇒	*rIPS* ⇒	*dlPFC* ⇒	*lMC* ⇒	*rMC* ⇒
dlPFC	1	1	1	1	1	0	0
lMC	0	1	0	1	1	1	1
rMC	0	1	1	0	1	1	1
DCM 17							
vmPFC	1	1	1	1	1	0	0
dmPFC	1	1	1	1	1	0	0
lIPS	1	1	1	1	1	0	0
rIPS	1	1	1	1	1	0	0
dlPFC	1	1	1	1	1	0	0
lMC	0	1	1	1	0	1	1
rMC	0	1	1	1	0	1	1
DCM 18							
vmPFC	1	1	1	1	1	0	0
dmPFC	1	1	1	1	1	0	0
lIPS	1	1	1	1	0	0	0
rIPS	1	1	1	1	0	0	0
dlPFC	1	1	1	1	1	0	0
lMC	0	1	1	1	1	1	1
rMC	0	1	1	1	1	1	1
DCM 19							
vmPFC	1	1	1	1	1	0	0
dmPFC	1	1	1	1	1	0	0
lIPS	1	1	1	1	1	0	0
rIPS	1	1	1	1	1	0	0
dlPFC	1	1	1	1	1	0	0
lMC	0	0	0	0	1	1	1
rMC	0	0	0	0	1	1	1
DCM 20							
vmPFC	1	1	1	1	1	0	0
dmPFC	1	1	0	0	0	0	0
lIPS	1	0	1	0	0	0	0
rIPS	1	0	0	1	0	0	0
dlPFC	1	0	0	0	0	0	0
lMC	0	1	1	1	1	1	1
rMC	0	1	1	1	1	1	1

Connection directionality moves from columns to rows as the arrows indicate. Existing connections are represented by ones, whereas zeros indicate no connection between regions. DCM, dynamic causal modeling.

Table S5. Fixed coupling parameters for the most likely dynamic causal model

	vmPFC ⇒	*dmPFC* ⇒	*lIPS* ⇒	*rIPS* ⇒	*dlPFC* ⇒	*lMC* ⇒	*rMC* ⇒
vmPFC	−1	**0.05** (σ^2 = 0.19e^{-3}; P_c = 1)	**0.06** (σ^2 = 0.18e^{-3}; P_c = 1)	**0.04** (σ^2 = 0.18e^{-3}; P_c = 1)	**0.03** (σ^2 = 0.19e^{-3}; P_c = 0.99)	—	—
dmPFC	**0.03** (σ^2 = 0.18e^{-3}; P_c = 0.99)	−1	**0.05** (σ^2 = 0.16e^{-3}; P_c = 1)	**0.02** (σ^2 = 0.16e^{-3}; P_c = 0.96)	**0.03** (σ^2 = 0.18e^{-3}; P_c = 0.98)	—	—
lIPS	**0.03** (σ^2 = 0.18e^{-3}; P_c = 0.99)	0.01 (σ^2 = 0.18e^{-3}; P_c = 0.8)	−1	0.01 (σ^2 = 0.17e^{-3}; P_c = 0.84)	**0.03** (σ^2 = 0.18e^{-3}; P_c = 0.98)	—	—
rIPS	**0.03** (σ^2 = 0.18e^{-3}; P_c = 0.98)	**0.02** (σ^2 = 0.18e^{-3}; P_c = 0.96)	**0.05** (σ^2 = 0.17e^{-3}; P_c = 1)	−1	**0.02** (σ^2 = 0.18e^{-3}; P_c = 0.96)	—	—
dlPFC	0.02 (σ^2 = 0.17e^{-3}; P_c = 0.89)	**0.02** (σ^2 = 0.18e^{-3}; P_c = 0.95)	**0.03** (σ^2 = 0.16e^{-3}; P_c = 0.98)	0 (σ^2 = 0.17e^{-3}; P_c = 0.61)	−1	—	—
lMC	—	**0.02** (σ^2 = 0.19e^{-3}; P_c = 0.91)	**0.03** (σ^2 = 0.18e^{-3}; P_c = 0.97)	**0.02** (σ^2 = 0.17e^{-3}; P_c = 0.93)	**0.02** (σ^2 = 0.19e^{-3}; P_c = 0.93)	−1	−0.01 (σ^2 = 0.18e^{-3}; P_c = 0.79)
rMC	—	**0.04** (σ^2 = 0.18e^{-3}; P_c = 1)	−0.01 (σ^2 = 0.18e^{-3}; P_c = 0.65)	0 (σ^2 = 0.17e^{-3}; P_c = 0.56)	**0.03** (σ^2 = 0.19e^{-3}; P_c = 0.98)	**−0.02** (σ^2 = 0.18e^{-3}; P_c = 0.94)	−1

Each cell provides statistics for the connection from the column area to the row area. σ^2, sample variance; P, probability that the specified input drives activity in the given region; P_c, probability that the absolute value of the coupling parameter is greater than zero [note that the absolute magnitude of coupling parameters is relative to the driving inputs and will change based on the scale of any parametric modulator (e.g., stimulus value) used as a driving input to the model]; P_m, probability that the coupling parameter is modulated by task condition. The effect size for these parameters should be evaluated relative to the magnitude of the fixed coupling parameters. Parameters with a posterior probability greater than 90% are shown in bold. All values are rounded to two decimals.

Table S6. Modulation of coupling parameters at initial options presentation

	vmPFC ⇒	*dmPFC* ⇒	*lIPS* ⇒	*rIPS* ⇒	*dlPFC* ⇒	*lMC* ⇒	*rMC* ⇒
vmPFC	**0.02** (σ^2 = 0.2e^{-3}; P_m = 0.93)	0 (σ^2 = 0.2e^{-3}; P_m = 0.62)	0 (σ^2 = 0.2e^{-3}; P_m = 0.63)	0 (σ^2 = 0.2e^{-3}; P_m = 0.57)	0 (σ^2 = 0.2e^{-3}; P_m = 0.63)	—	—
dmPFC	**0.02** (σ^2 = 0.19e^{-3}; P_m = 0.93)	0.01 (σ^2 = 0.2e^{-3}; P_m = 0.77)	0 (σ^2 = 0.2e^{-3}; P_m = 0.57)	0 (σ^2 = 0.2e^{-3}; P_m = 0.51)	0.01 (σ^2 = 0.2e^{-3}; P_m = 0.79)	—	—
lIPS	**0.03** (σ^2 = 0.19e^{-3}; P_m = 0.97)	0 (σ^2 = 0.2e^{-3}; P_m = 0.51)	0.02 (σ^2 = 0.2e^{-3}; P_m = 0.89)	0.01 (σ^2 = 0.2e^{-3}; P_m = 0.71)	0.01 (σ^2 = 0.2e^{-3}; P_m = 0.8)	—	—
rIPS	**0.02** (σ^2 = 0.19e^{-3}; P_m = 0.95)	0 (σ^2 = 0.2e^{-3}; P_m = 0.6)	0.01 (σ^2 = 0.2e^{-3}; P_m = 0.76)	0.02 (σ^2 = 0.2e^{-3}; P_m = 0.88)	0.01 (σ^2 = 0.2e^{-3}; P_m = 0.71)	—	—
dlPFC	0 (σ^2 = 0.19e^{-3}; P_m = 0.59)	0 (σ^2 = 0.2e^{-3}; P_m = 0.63)	0 (σ^2 = 0.2e^{-3}; P_m = 0.58)	0 (σ^2 = 0.2e^{-3}; P_m = 0.51)	0.01 (σ^2 = 0.2e^{-3}; P_m = 0.74)	—	—
lMC	—	0 (σ^2 = 0.2e^{-3}; P_m = 0.63)	0 (σ^2 = 0.2e^{-3}; P_m = 0.62)	0 (σ^2 = 0.2e^{-3}; P_m = 0.63)	0.01 (σ^2 = 0.2e^{-3}; P_m = 0.78)	0 (σ^2 = 0.2e^{-3}; P_m = 0.59)	0 (σ^2 = 0.2e^{-3}; P_m = 0.54)
rMC	—	0.01 (σ^2 = 0.2e^{-3}; P_m = 0.74)	0 (σ^2 = 0.2e^{-3}; P_m = 0.58)	0.01 (σ^2 = 0.2e^{-3}; P_m = 0.65)	0.01 (σ^2 = 0.2e^{-3}; P_m = 0.81)	0 (σ^2 = 0.2e^{-3}; P_m = 0.53)	0 (σ^2 = 0.2e^{-3}; P_m = 0.63)

Each cell provides statistics for the connection from the column area to the row area. σ^2, sample variance; P, probability that the specified input drives activity in the given region; P_c, probability that the absolute value of the coupling parameter is greater than zero [note that the absolute magnitude of coupling parameters is relative to the driving inputs and will change based on the scale of any parametric modulator (e.g., stimulus value) used as a driving input to the model]; P_m, probability that the coupling parameter is modulated by task condition. The effect size for these parameters should be evaluated relative to the magnitude of the fixed coupling parameters. Parameters with a posterior probability greater than 90% are shown in bold. All values are rounded to two decimals.

Table S7. Modulation of coupling parameters by choice during the period from stimulus onset to response conditional on left choice

	vmPFC ⇒	*dmPFC ⇒*	*lIPS ⇒*	*rIPS ⇒*	*dlPFC ⇒*	*lMC ⇒*	*rMC ⇒*
vmPFC	**0.02** (σ^2 = 0.19e^{-3}; P_m = 0.92)	0.02 (σ^2 = 0.19e^{-3}; P_m = 0.88)	0.02 (σ^2 = 0.19e^{-3}; P_m = 0.89)	0.01 (σ^2 = 0.19e^{-3}; P_m = 0.86)	0.01 (σ^2 = 0.2e^{-3}; P_m = 0.8)	—	—
dmPFC	0.01 (σ^2 = 0.19e^{-3}; P_m = 0.78)	**0.02** (σ^2 = 0.2e^{-3}; P_m = 0.96)	**0.02** (σ^2 = 0.18e^{-3}; P_m = 0.92)	0.01 (σ^2 = 0.18e^{-3}; P_m = 0.8)	**0.02** (σ^2 = 0.19e^{-3}; P_m = 0.9)	—	—
lIPS	0.01 (σ^2 = 0.19e^{-3}; P_m = 0.83)	0.01 (σ^2 = 0.19e^{-3}; P_m = 0.79)	**0.04** (σ^2 = 0.19e^{-3}; P_m = 0.99)	0.01 (σ^2 = 0.19e^{-3}; P_m = 0.8)	0.01 (σ^2 = 0.19e^{-3}; P_m = 0.84)	—	—
rIPS	0.01 (σ^2 = 0.19e^{-3}; P_m = 0.77)	0.01 (σ^2 = 0.19e^{-3}; P_m = 0.79)	**0.02** (σ^2 = 0.19e^{-3}; P_m = 0.97)	**0.03** (σ^2 = 0.19e^{-3}; P_m = 0.99)	0.01 (σ^2 = 0.19e^{-3}; P_m = 0.77)	—	—
dlPFC	0 (σ^2 = 0.18e^{-3}; P_m = 0.56)	0.01 (σ^2 = 0.19e^{-3}; P_m = 0.73)	0.01 (σ^2 = 0.18e^{-3}; P_m = 0.7)	0 (σ^2 = 0.19e^{-3}; P_m = 0.6)	0.02 (σ^2 = 0.2e^{-3}; P_m = 0.86)	—	—
lMC	—	**−0.03** (σ^2 = 0.19e^{-3}; P_m = 0.97)	**−0.02** (σ^2 = 0.18e^{-3}; P_m = 0.97)	**−0.02** (σ^2 = 0.19e^{-3}; P_m = 0.93)	−0.01 (σ^2 = 0.19e^{-3}; P_m = 0.79)	0.01 (σ^2 = 0.2e^{-3}; P_m = 0.73)	−0.02 (σ^2 = 0.2e^{-3}; P_m = 0.88)
rMC	—	**0.04** (σ^2 = 0.19e^{-3}; P_m = 1)	**0.02** (σ^2 = 0.19e^{-3}; P_m = 0.92)	**0.03** (σ^2 = 0.19e^{-3}; P_m = 0.97)	**0.02** (σ^2 = 0.19e^{-3}; P_m = 0.96)	0.01 (σ^2 = 0.2e^{-3}; P_m = 0.7)	**0.04** (σ^2 = 0.2e^{-3}; P_m = 1)

Each cell provides statistics for the connection from the column area to the row area. σ^2, sample variance; P, probability that the specified input drives activity in the given region; P_c, probability that the absolute value of the coupling parameter is greater than zero [note that the absolute magnitude of coupling parameters is relative to the driving inputs and will change based on the scale of any parametric modulator (e.g., stimulus value) used as a driving input to the model]; P_m, probability that the coupling parameter is modulated by task condition. The effect size for these parameters should be evaluated relative to the magnitude of the fixed coupling parameters. Parameters with a posterior probability greater than 90% are shown in bold. All values are rounded to two decimals.

Table S8. Modulation of coupling parameters by choice during the period from stimulus onset to response conditional on right choice

	vmPFC ⇒	*dmPFC ⇒*	*lIPS ⇒*	*rIPS ⇒*	*dlPFC ⇒*	*lMC ⇒*	*rMC ⇒*
vmPFC	0.02 (σ^2 = 0.19e^{-3}; P_m = 0.89)	**0.02** (σ^2 = 0.19e^{-3}; P_m = 0.93)	**0.03** (σ^2 = 0.19e^{-3}; P_m = 0.98)	0.02 (σ^2 = 0.19e^{-3}; P_m = 0.87)	0.01 (σ^2 = 0.2e^{-3}; P_m = 0.85)	—	—
dmPFC	0.02 (σ^2 = 0.19e^{-3}; P_m = 0.89)	**0.02** (σ^2 = 0.19e^{-3}; P_m = 0.95)	0.02 (σ^2 = 0.18e^{-3}; P_m = 0.87)	0 (σ^2 = 0.18e^{-3}; P_m = 0.55)	0.01 (σ^2 = 0.19e^{-3}; P_m = 0.69)	—	—
lIPS	0.01 (σ^2 = 0.19e^{-3}; P_m = 0.83)	0 (σ^2 = 0.19e^{-3}; P_m = 0.56)	**0.03** (σ^2 = 0.19e^{-3}; P_m = 0.99)	0 (σ^2 = 0.19e^{-3}; P_m = 0.5)	0.01 (σ^2 = 0.19e^{-3}; P_m = 0.68)	—	—
rIPS	0.02 (σ^2 = 0.19e^{-3}; P_m = 0.89)	0.01 (σ^2 = 0.19e^{-3}; P_m = 0.7)	**0.02** (σ^2 = 0.18e^{-3}; P_m = 0.92)	**0.04** (σ^2 = 0.19e^{-3}; P_m = 1)	0.01 (σ^2 = 0.19e^{-3}; P_m = 0.7)	—	—
dlPFC	0.01 (σ^2 = 0.18e^{-3}; P_m = 0.8)	0.01 (σ^2 = 0.19e^{-3}; P_m = 0.78)	0.01 (σ^2 = 0.17e^{-3}; P_m = 0.77)	0 (σ^2 = 0.19e^{-3}; P_m =0.58)	0.01 (σ^2 = 0.19e^{-3}; P_m = 0.86)	—	—
lMC	—	**0.04** (σ^2 = 0.19e^{-3}; P_m = 1)	**0.05** (σ^2 = 0.19e^{-3}; P_m = 1)	**0.04** (σ^2 = 0.19e^{-3}; P_m = 0.99)	**0.03** (σ^2 = 0.19e^{-3}; P_m = 0.98)	**0.03** (σ^2 = 0.2e^{-3}; P_m = 0.99)	0.01 (σ^2 = 0.2e^{-3}; P_m = 0.75)
rMC	—	−0.01 (σ^2 = 0.19e^{-3}; P_m = 0.64)	**−0.02** (σ^2 = 0.19e^{-3}; P_m = 0.96)	**−0.02** (σ^2 = 0.18e^{-3}; P_m = 0.94)	0 (σ^2 = 0.19e^{-3}; P_m = 0.61)	−0.02 (σ^2 = 0.2e^{-3}; P_m = 0.88)	0.01 (σ^2 = 0.2e^{-3}; P_m = 0.69)

Each cell provides statistics for the connection from the column area to the row area. σ^2, sample variance; P, probability that the specified input drives activity in the given region; P_c, probability that the absolute value of the coupling parameter is greater than zero [note that the absolute magnitude of coupling parameters is relative to the driving inputs and will change based on the scale of any parametric modulator (e.g., stimulus value) used as a driving input to the model]; P_m, probability that the coupling parameter is modulated by task condition. The effect size for these parameters should be evaluated relative to the magnitude of the fixed coupling parameters. Parameters with a posterior probability greater than 90% are shown in bold. All values are rounded to two decimals.

Table S9. Modulation of coupling parameters at the time of response

	vmPFC ⇒	*dmPFC* ⇒	*lIPS* ⇒	*rIPS* ⇒	*dlPFC* ⇒	*lMC* ⇒	*rMC* ⇒
vmPFC	—	—	—	—	—	—	—
dmPFC	—	—	—	—	—	—	—
lIPS	—	—	—	—	—	—	—
rIPS	—	—	—	—	—	—	—
dlPFC	—	—	—	—	—	—	—
lMC	—	—	—	—	—	0.01 ($\sigma^2 = 0.2e^{-3}$; $P_m = 0.76$)	0 ($\sigma^2 = 0.2e^{-3}$; $P_m = 0.55$)
rMC	—	—	—	—	—	0 ($\sigma^2 = 0.2e^{-3}$; $P_m = 0.58$)	0.01 ($\sigma^2 = 0.2e^{-3}$; $P_m = 0.76$)

Each cell provides statistics for the connection from the column area to the row area. σ^2, sample variance; *P*, probability that the specified input drives activity in the given region; P_c, probability that the absolute value of the coupling parameter is greater than zero [note that the absolute magnitude of coupling parameters is relative to the driving inputs and will change based on the scale of any parametric modulator (e.g., stimulus value) used as a driving input to the model]; P_m, probability that the coupling parameter is modulated by task condition. The effect size for these parameters should be evaluated relative to the magnitude of the fixed coupling parameters. Parameters with a posterior probability greater than 90% are shown in bold. All values are rounded to two decimals.

Table S10. Parameter estimates for each task related input by region

	Stimulus presentation	Stimulus value	CR left	CR right	Button press
vmPFC	**−0.01** ($\sigma^2 = 0.01e^{-3}$; $P = 0.9$)	**0.04** ($\sigma^2 = 0.23e^{-3}$; $P = 0.99$)	—	—	—
dmPFC	—	—	**0.01** ($\sigma^2 = 0e^{-3}$; $P = 1$)	**0.01** ($\sigma^2 = 0e^{-3}$; $P = 1$)	—
lIPS	—	—	**0.01** ($\sigma^2 = 0e^{-3}$; $P = 1$)	**0.01** ($\sigma^2 = 0e^{-3}$; $P = 1$)	—
rIPS	—	—	**0.01** ($\sigma^2 = 0e^{-3}$; $P = 1$)	**0.01** ($\sigma^2 = 0e^{-3}$; $P = 1$)	—
dlPFC	**−0.01** ($\sigma^2 = 0.01e^{-3}$; $P = 0.99$)	—	**0.01** ($\sigma^2 = 0e^{-3}$; $P = 1$)	**0.01** ($\sigma^2 = 0e^{-3}$; $P = 1$)	—
lMC	—	—	—	—	**0.07** ($\sigma^2 = 0.14e^{-3}$; $P = 1$)
rMC	—	—	—	—	**0.07** ($\sigma^2 = 0.17e^{-3}$; $P = 1$)

Each cell provides statistics for the connection from the column area to the row area. σ^2, sample variance; *P*, probability that the specified input drives activity in the given region; P_c, probability that the absolute value of the coupling parameter is greater than zero [note that the absolute magnitude of coupling parameters is relative to the driving inputs and will change based on the scale of any parametric modulator (e.g., stimulus value) used as a driving input to the model]; P_m, probability that the coupling parameter is modulated by task condition. The effect size for these parameters should be evaluated relative to the magnitude of the fixed coupling parameters. Parameters with a posterior probability greater than 90% are shown in bold. All values are rounded to two decimals.

Table S11. Regions correlated with right and left value across all trials

Region	BA	Side	Cluster size	*x*	*y*	*z*	*Z* score
Region correlated with left value							
Precentral gyrus	3/4	Right	179	48	−19	64	4.15*
Region correlated with right value							
Precentral gyrus	6/4/3	Left	1,073	−42	−19	61	4.88*
Medial frontal gyrus	9/8	Right	176	24	29	37	4.45*
Rolandic operculum/insula	13	Left	149	−42	−28	19	4*
Inferior frontal gyrus	10/46	Right	25	48	53	4	3.67
Middle temporal gyrus	39	Right	21	45	−82	25	3.64
Cerebellum		Right	57	12	−85	−29	3.58
Orbitofrontal cortex	10	Left	37	−21	50	−5	3.51
Occipital cortex	19	Left	20	−12	−97	34	3.09

Height threshold $t = 2.88$; extent threshold = 20 voxels ($3 \times 3 \times 3$ mm). BA, Brodmann area.
*The activation survives whole-brain correction for multiple comparisons at the cluster level (height threshold $t = 2.88$, extent = 178 voxels for the left value, extent = 122 voxels for the right value).